

Ram Accelerator Direct Space Launch System: New Concepts

David W. Bogdanoff*

Eloret Institute, Palo Alto, California 94303

The ram accelerator, a chemically driven ramjet-in-tube device is a new option for direct launch of acceleration-insensitive payloads into Earth orbit. The projectile is the centerbody of a ramjet and travels through a tube filled with a premixed fuel-oxidizer mixture. The tube acts as the cowl of the ramjet. A number of new concepts for a ram accelerator space launch system are presented. The velocity and acceleration capabilities of a number of ram accelerator drive modes, including several new modes, are given. Passive (fin) stabilization during atmospheric transit is investigated and found to be promising. Gasdynamic heating in-tube and during atmospheric transit is studied; the former is found to be severe, but may be alleviated by the selection of the most suitable drive modes, transpiration cooling, or a hydrogen gas core in the launch tube. To place the payload in Earth orbit, scenarios using one impulse and three impulses (with an aeropass) and a new scenario involving an auxiliary vehicle are studied. The auxiliary vehicle scenario is found to be competitive regarding payload, and requires a much simpler projectile, but has the disadvantage of requiring the auxiliary vehicle.

I. Introduction

THE establishment of a large-scale space presence and, in particular, substantial space manufacturing systems and the exploration and colonization of the solar system would benefit greatly from a more economical access to space. The current high cost of space access is a significant barrier to the realization of the above concepts. Much of the material to be transferred from Earth to space, such as rocket propellants, water, raw materials for space manufacture, and components of large space structures is insensitive to acceleration. A number of high-acceleration schemes for direct launch into space from the Earth's surface have been proposed.¹⁻¹⁴ These include hypervelocity guns,^{1,2} various electromagnetic launchers,³⁻⁷ and beamed energy concepts.¹¹⁻¹⁴

Hypervelocity guns have very uneven acceleration histories and low efficiencies. There are severe problems in handling the large instantaneous electrical powers required by the proposed electromagnetic launchers. Beamed energy concepts encounter severe problems in atmospheric transmission, maintaining the required beam focus and tracking the vehicle with the required accuracy. These concepts, in general, encounter substantial problems in scaling up to sizes useful to direct launch.

At the University of Washington, a chemical energy-based ramjet-in-tube (hereafter, "ram accelerator") has been developed for efficiently launching large payloads (up to several metric tons) directly into space from the Earth's surface.¹⁵⁻²² The projectile is the centerbody of a ramjet and travels through a tube filled with a premixed fuel-oxidizer mixture. The tube acts as the cowl of the ramjet. The composition, speed of sound, and pressure of the working gas can be controlled to produce a nearly constant projectile acceleration over the full operating velocity range. This concept can almost certainly be scaled from grams to thousands of kilograms and offers the potential for the direct launch into space of acceleration-insensitive payloads.²³⁻²⁴ (As an example of scaling to large sizes, during World War II the German army used two artill-

ery pieces²⁵ with 0.80-m bore capable of launching 7000-kg projectiles to muzzle velocities of 0.7 km/s.

11. Ram Accelerator Drive Modes

A number of drive modes for the ram accelerator have been investigated. Five modes have been described in Refs. 15 and 17. Here, we briefly review the modes most applicable to a space launch system and describe three new modes. Five modes are shown in Fig. 1, where CL denotes centerline, S shock wave, C combustion zone, CP choke point, D detonation wave, and M Mach number. Wiggly lines denote the beginning of the combustion zone. Figure 1a shows the thermally choked subsonic combustion (TC) mode. The forward part of the projectile is a supersonic diffuser. The flat base of the projectile serves as a flame-holding dump combustor, acting in a very similar way to the v-gutter flameholders discussed in Ref. 26. The heat release chokes the flow behind the projectile and maintains the normal shock wave on the tapering rear part of the projectile. Experimental data from Refs. 21 and 22 suggest the existence of a new mode, the variant of the TC mode shown in Fig. 1b (TCV mode). In this mode, the projectile velocity is near to or above the detonation velocity of the working gas. Downstream of the projectile throat the flow is decelerated through a complex system of shocks²⁷ similar to those comprising a "normal shock" in a duct. Because of the velocity range, temperatures in the shock system cause ignition and there is substantial heat release on the projectile. The heat release continues past the projectile rear and thermally chokes the flow at CP. The flow which is thermally choked occupies significantly less than full-tube area and stands adjacent to a low-speed separated flow zone. (The above description is based, in part, on Refs. 21 and 22, where it is stated that, in this velocity range, 1) heat release is believed to occur at least partially on the projectile body, and 2) the propulsion mode may not require thermal choking at full-tube area to stabilize the driving pressure wave system on the projectile.) A possible variant of this mode would be to have the choke point move forward and to reside on the tapering projectile rear.

An oblique detonation (OD1) mode is shown in Fig. 1c. In this mode, the flow is supersonic throughout and the working gas composition, the projectile velocity, and the projectile nose geometry are such that the bow shock does not initiate

Received Oct. 11, 1990; revision received April 26, 1991; accepted for publication April 29, 1991. Copyright © 1991 by the American Institute of Aeronautics and Astronautics, Inc. All rights reserved.

*Senior Research Scientist. Mailing address: NASA Ames Research Center, Mail stop 230-2, Moffett Field, CA 94035. Associate Fellow AIAA.

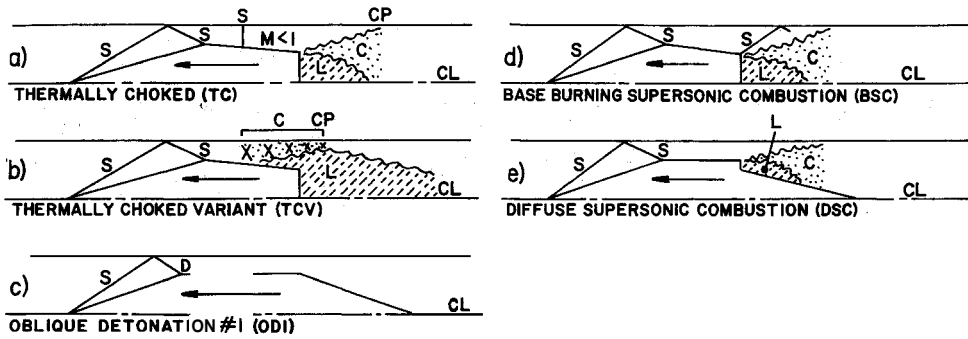


Fig. 1 Some operating modes of the ram accelerator. *S*, shock wave; *C*, combustion zone; *L*, low-velocity flow zone; *CP*, choke point; *D*, detonation wave; *M*, Mach number. Wiggly lines denote edge of combustion and/or low-velocity flow zones. Heavy crosses represent a complex shock system.

combustion but its reflected shock does. In a second oblique detonation (OD2) mode (not shown), the initial compression is more gradual and does not initiate combustion. Combustion is initiated by a small, but steep ramp on the projectile. Both OD modes likely have variants where combustion does not take place immediately behind the initiating shock (as in a detonation) but is instead delayed and takes place a significant distance behind the shock. For a limited range of working gas mixtures and projectile geometries, axisymmetric CFD calculations^{18,20} show operating velocity ranges for the OD1 and OD2 modes of 3.1–9.5 and 4.1–9.9 km/s, respectively.

Two new modes are shown in Fig. 1, d and e. Figure 1d shows the base burning supersonic combustion (BSC) mode. This mode was first described by Kepler.²⁸ This mode resembles the TC mode, except that there is no normal shock on the projectile and the outer flow is supersonic throughout. For this mode to generate thrust, the high pressures generated aft of the projectile by combustion must propagate forward through the subsonic wake region and bear on the base of the projectile. Finally, Fig. 1e shows the diffuse supersonic combustion (DSC) mode. In this mode, combustion takes place in the nozzle expansion region and a small rearward-facing step is shown as one way to anchor the combustion front. One-dimensional theoretical analyses, outlined in Appendix A, give operating velocity ranges for these modes of 1.5–11 km/s.

The TC mode has been demonstrated experimentally at the University of Washington over a velocity range of 0.7–2.4 km/s.^{15,16,19} Projectiles with a diameter of 3.8 cm and masses of 45–75 g were used. With initial tube gas fill pressures of –20 atm, accelerations of 15,000–30,000 g were obtained. Theoretical analyses^{15,16,19} show that the TC mode can operate up to the detonation velocity of the working gas. Operation of the ram accelerator at velocities bracketing and above the working gas detonation velocity is reported in Refs. 22 and 21, respectively. The data of these references suggest operation in the TCV mode in the lower velocity ranges and the TCV mode in combination with the OD1 (or possibly OD2) modes in the higher velocity ranges. However, it is clear that much work remains to be done before it can be said that experimental ram accelerator operation near and above the working gas detonation velocity is well understood. One-dimensional analyses, similar to those described in Appendix A, indicate that the TCV mode can operate up to two or more times the working gas detonation velocity.

In comparing among the various modes, an important parameter is the thrust pressure ratio, R_p . R_p is equal to p_{dr}/P_{max} where p_{dr} is defined by $p_{dr} = (am)/A_0$, where a is the projectile acceleration and m and A_0 are the mass and the maximum area of the projectile, respectively, and P_{max} is the maximum cycle pressure. For similar projectile materials and design, the projectile mass tends to be proportional to P_{max} , since the (generally hollow) projectile must withstand the maximum crushing pressures produced in the projectile drive mode. The projectile drive force is proportional to p_{dr} . We

define C_k as the kinetic energy capability, $(v_2^2 - v_1^2)/2$, of a length s of ram accelerator tube. (v_1 and v_2 are the projectile entrance and exit velocities, respectively, for the length of tube in question.) C_k is, then, proportional to R_p , ($= p_{dr}/P_{max}$) and s . Higher R_p values are desirable since they allow given velocities to be achieved in shorter tube lengths.

There are important differences among the R_p values of the various modes. Experimental values^{15,19} of R_p for the TC mode range from 0.50 to 0.75. Theoretical values^{17,18,20} of R_p for the OD1 and OD2 modes are 0.12–0.15 and 0.17–0.20, respectively. Experimentally, $R_p = 0.22$ –0.38 and $R_p = 0.25$ for operation bracketing²² and above²¹ the detonation velocity, respectively [exact mode(s) not yet clear]. From the simple analyses outlined in Appendix A, R_p for the BSC and DSC modes can be estimated to be 0.6–0.7 and –0.4, respectively. The higher R_p values of the DSC and BSC modes are due primarily to reductions in the maximum cycle pressure which, in turn, follows from the absence of detonation waves and combustion in a flow area larger than those for the OD1 and OD2 modes.

111. Launch Tube Concepts

A. Preliminary Discussion

References 23 and 24 discuss a ram accelerator space transportation system in some detail. The mission scenario therein is a 2000-kg projectile to be delivered to a 400-km space station orbit. Reference 24 estimates payload fractions of 19–43%. A muzzle velocity of 8–10 km/s is required and the projectile acceleration is limited to –1000 g; this results in a launch tube length of 3–5 km. The projectile length, diameter, and forward and rear cone angles are 7.5 m, 76 cm, and 7 deg, respectively (from Ref. 24). The maximum cycle pressures are 2000–4000 atm. Our work here will be referenced to the same mission scenario and we will take this projectile to be our "standard" projectile.

B. Fins on Projectile or Rails on Tube

The projectile is very likely to be unstable in the launch tube²⁴ and, if so, must be stabilized by fins on the projectile or rails on the tube. For a small-scale research tool, the advantages of tube simplicity and readily variable area ratio weigh heavily in favor of fins on the projectile. Another advantage is that the forward part of the flow can be made perfectly axisymmetric. However, once the desired area ratios have been determined, for a large-scale launch system, the advantages of mass savings (no sabot or fins), absence of sabot stripper, and the possibility of variable area ratio along the tube are heavily in favor of rails on the tube. However, for this case, the forward part of the flow pattern cannot be made axisymmetric. It is possible that interactions of the projectile bow shock with the rails could interfere with the proper operation of the desired mode or cause localized projectile ablation. Also, the rails could cause wear grooves in the projectile.

Should these problems prove serious, fins on the projectile might be necessary for a large-scale launch system.

C. Use of Thermally Choked Mode

In Refs. 23 and 24, the launch scenario involves acceleration in a gun from 0 to 0.7 km/s, followed by acceleration using the TC mode up to 2.5–3.0 km/s and, finally, acceleration using the OD1 or OD2 modes up to 8–10 km/s. A new, alternative scenario is to use the gun to accelerate up to -2.0 km/s and then go directly to above detonation velocity operation. The initial accelerator could be a combustion-powered gun. Reference 29 reports the acceleration of projectiles to 2.3–3.8 km/s in a 4-cm gun driven by a $3\text{H}_2 + \text{O}_2 + 8\text{He}$ combustion mixture. Reference 30 reports the acceleration of a relatively light projectile to -2.1 km/s in a 36-cm gun driven by a $7\text{H}_2 + \text{O}_2$ mixture. The new scenario has the advantages that: 1) the projectile geometry can be optimized for operation above the detonation velocity, 2) no diaphragm is needed between TC and above detonation velocity sections of the launch tube, and 3) no ignition system is required for the TC mode. [We note that many above detonation velocity modes (particularly the OD1 and OD2 modes) should not require ignition systems.] A disadvantage of the new scenario is that the required accelerations in the initial accelerator are higher and this will tend to make the projectile somewhat more massive.

IV. Projectile Stability

The basic projectile of Ref. 24 (shown in Fig. 2) is unstable in flight through the atmosphere. Spinning the projectile or the use of active stability augmentation devices are possible ways to deal with this problem. Spinning may well not be effective for such a long, slender projectile because of the very high spin rates necessary to overcome the aerodynamic pitching moments and the consequent destabilizing Magnus forces and moments. Spinning would leave the projectile in space with a very high spin rate, making contact and cargo transfer extremely awkward, to say the least, unless an active despin system was included aboard the projectile. Active stabilization has the disadvantages of high cost (on projectiles that are likely to be expendable), complexity and consequent reliability concerns (especially given the initial high g environment) and added projectile mass.

A new concept is the possible passive stabilization using cruciform fins. Several possible geometries are shown conceptually in Fig. 3. We do not attempt to estimate the stability parameters of these projectiles; rather we will assume that they can be made at least as stable as certain projectiles for which experimental hypersonic stability data are available. Stability data on small 10-deg half-angle tantalum-aluminum cones at Mach 15 in air are presented in Ref. 31. Equations relating such stability data to the wavelength (λ) and the envelope of the amplitude (a_e) of the pitch oscillations are given in Ref. 32. The envelope of the maximum angular velocity or rate of change of pitch angle (\dot{a}_e) follows directly from λ , a_e , and the projectile velocity. The equations and analyses used are reviewed briefly in Appendix B.

The dynamics of these small projectiles can readily be scaled to a 2000-kg ram accelerator projectile and the proper velocity and atmospheric density profile. A representative ram accelerator mission, launch at 7 km/s and 20-deg angle from a 4-km altitude, is chosen for stability analysis. The following

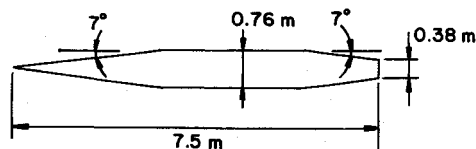


Fig. 2 Basic ram accelerator space launch projectile of Ref. 24. Total projectile mass = 2000 kg.

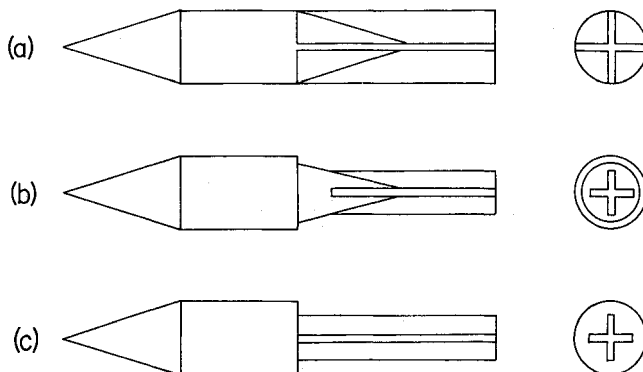


Fig. 3 Side and rear views of projectiles with stabilizing fins: a) for OD1 or OSIC1 mode; b) for DSC mode; c) for BSC mode.

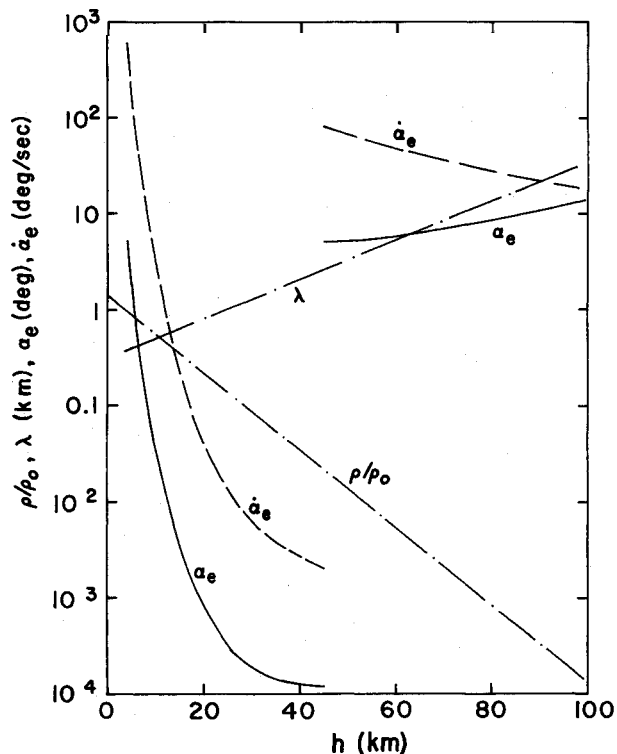


Fig. 4 Stability parameters for 2000-kg 10-deg half-angle conical projectile launched from 4-km altitude at 20 deg from horizontal and 7 km/s. ρ/ρ_0 is (air density)/(launch air density) ratio, λ is pitch oscillation wavelength (km), a_e is envelope of maximum pitch angle (deg), \dot{a}_e is the envelope of maximum pitch rate (deg/s). Also, see text.

simplifying assumptions are made: flat, nonrotating Earth; exponential density decrease with altitude; no gravity; and projectile velocity constant at 7 km/s. These assumptions should have only minor effects on the projectile stability characteristics.

Figure 4 shows the resulting plots of λ , a_e , \dot{a}_e , and ρ/ρ_0 versus altitude h . (ρ is the air density and ρ_0 is ρ at the launch elevation, 4 km.) λ and ρ/ρ_0 vary exponentially with altitude. For h from 4 to 45 km, the a_e and \dot{a}_e curves are drawn assuming that the projectile was disturbed to produce $a_e = 5$ deg at $h = 5$ km. The pitch oscillations are seen to be rapidly damped out. Above 45 km, the projectile is unstable in pitch, but with a very slowly increasing pitch amplitude. For h from 45 to 96 km, the a_e and \dot{a}_e curves are drawn assuming that the projectile was disturbed to produce $a_e = 5$ deg at $h = 45$ km. a_e increases very slowly from 45 to 96 km altitude and \dot{a}_e continues to decrease with increasing altitude. At $h = 96$ km, the atmosphere is very thin and λ is of the same magnitude as the length, along the projectile path, over which the at-

atmospheric density decreases by a factor of e . An estimate of the final free tumbling rate of the projectile in space is $\dot{\alpha}_e$ at $h = 96$ km, which is -20 deg/s or -3.2 rpm. If $\dot{\alpha}_e$ at 45 km was less, say, 2 deg, the final tumbling rate would be -1.3 rpm. At these low tumbling rates, there should be little difficulty in making contact with and transferring cargo from the projectile.

Fin stabilization also offers the possibility that the projectile might be stable in the tube without being in contact with the wall.

V. Gasdynamic Heating

A. Ablation and Transpiration Cooling Requirements

Heating rates and ablation or transpiration cooling requirements were investigated for three critical regions of the projectile: the nose, both in-tube and during atmospheric transit; the forward cone during atmospheric transit; and the maximum pressure region of the projectile in-tube. This problem has been discussed earlier,^{23,24} but the present analyses are more detailed and reveal a problem not explicitly dealt with therein. The methods used to estimate the gasdynamic heating are outlined in Appendix C. Our standard projectile is used here and we have assumed an initial nose radius of 3.8 cm.

Two mission profiles were investigated. The parameters for each are given in Table 1. For each critical area of both missions, the mass consumed due to heat loading was calculated for carbon ablation and NH_3 and H, transpiration cooling. The ablatant would most likely be a carbon-carbon composite. Using hydrogen as the transpirant compared with ammonia requires 3–3.5 times less mass of transpirant but 2.6–3.1 times more volume of transpirant on account of the low density of liquid H. For this reason and the very low temperature required to store liquid H, hereafter we will consider carbon ablation and NH_3 transpiration cooling only.

For a noncryogenic, high-density transpirant, NH_3 was selected over water or hydrocarbons for the following reasons. As the transpirants flow through fine passages approaching the projectile surface, the temperature rises steeply. Equilibrium calculations were made for CH_4 , H_2O , and NH_3 transpirants at a representative pressure of 3000 atm. CH_4 was considered as representative for hydrocarbon transpirants. For CH_4 , a mole fraction of -0.0085 of graphite was found in the 1100–1500 K range. The graphite could plug fine transpiration passages. For water transpirant in the 3000–4000 K range, the mole fractions of O, and O range from 0.004–0.018 and 0.0001–0.0036, respectively. The presence of these species is likely to cause oxidation damage to the porous media. For NH_3 transpirant, the very chemically active species N is present in mole fractions of only 10^{-7} – 1.6×10^{-5} over the 3000–4000 K temperature range. Hence ammonia is preferred over hydrocarbons or water.

Table 2 gives our estimates of material loss (ablatant or transpirant) for the critical projectile regions for the moderate and severe missions. Three measures of material loss are used in Table 2. dMIM is the mass of the lost material divided by the initial projectile mass. For ablation, dlr is the projectile wall retreat divided by the maximum initial projectile radius, and r_f/r_i is the final nose radius divided by the initial nose radius (3.8 cm).

We first address nose carbon ablation mass loss. We go directly to the severe mission and make estimates of the total values of dMIM and $r_f/r_i - 1$ by adding the individual values for in-tube flight and atmospheric transit. The final value of r_f/r_i is 1.7 and of dMIM is 0.00104, corresponding to a loss of 2.1 kg of ablatant. This amount of ablation should have very little effect on the ability of the projectile to perform the mission. We now turn to C ablation on the forward cone during atmospheric transit, again going directly to the severe mission. dMIM is 0.0265, corresponding to 53 kg of carbon lost and dlr is 0.0241, corresponding to a wall retreat of 0.92

Table 1 Missions for the assessment of gasdynamic heating

Mission	Moderate	Severe
Drive mode	OD2	OD2
Gas mixture at tube exit	$8\text{H}_2 + \text{O}_2$	$8\text{H}_2 + \text{O}$
Velocity at tube exit, km/s	7	10
Tube fill pressure, atm	25	25
Launch angle, deg	20	20
Launch, altitude, km	4.5	0

Table 2 Estimates of material lost due to gasdynamic heating

Portion of total flight profile	Location on projectile	Material lost	Measure of material lost	Moderate mission	Severe mission
				(7 km/s)	(10 km/s)
In tube	Nose	C	r_f/r_i	1.016	1.300
		C	dMIM	0.000019	0.00043
		NH_3	dMIM	0.000054	0.00086
	Sidewall (at max. p)	C	dlr	0.025	0.203
		C	dMIM	0.050	0.407
		NH_3	dMIM	0.068	0.431
Atmosphere	Nose	C	r_f/r_i	1.047	1.409
		C	dMIM	0.000053	0.00061
		NH_3	dMIM	0.000150	0.00116
	Forward cone	C	dlr	0.0085	0.0241
		C	dMIM	0.0094	0.0265
		NH_3	dMIM	0.0092	0.0222

cm. If the ablation is axisymmetric, it seems likely that this amount of ablation is also acceptable, since maintaining the exact projectile shape is not critical during atmospheric transit.

Finally, we turn to in-tube projectile sidewall heating in the region of maximum pressure. Even for the moderate mission, ablation here is a serious problem. A wall retreat of 0.95 cm is predicted. This retreat in the critical high-pressure region of the flow could cause the projectile shape to be altered so that the drive mode does not operate properly. Further, assuming that rails or fins are required to stabilize the projectile, the projectile could lose contact with the tube, leading to violent oscillations and destruction of the projectile. For the severe mission, the wall retreat is predicted to be -8 times greater than for the moderate mission, almost certainly leading to projectile destruction early in in-tube flight.

Our calculations show that the BSC mode produces -10 times less ablation than the OD2 mode. This is because (ideally) the maximum cycle pressure applied to the projectile sidewall is very much lower, relative to the effective projectile driving pressure, for the BSC mode (see Sec. 11). Even partial achievement of the BSC (or, somewhat less good, DSC) mode operation would greatly reduce the amount of ablation. (We note here that the OD1 and OD2 modes produce similar severe ablation.) Let us examine the use of transpiration cooling with NH_3 . For the severe mission, the NH_3 transpirant required is 0.41 and 0.04 of the projectile initial mass, for the OD2 and BSC drive modes, respectively. A good option might be to use BSC or DSC drive operation and NH_3 transpiration cooling together.

B. Hydrogen Gas Core

A third, new method for reducing in-tube ablation is to use tangential gas injection and a vortex-stabilized hydrogen gas core in the tube; this can easily be shown to greatly reduce the heat transfer to the projectile. Even if the projectile is stable in the tube without fins or rails, operation with a vortex-stabilized hydrogen core is very awkward. The tube must have tangential injection ports along its entire length. Injection must take place simultaneously over the full-tube length, many different propellant gas mixtures must be injected (immediately following the injection of the hydrogen core), and gas injection and launch must be accomplished in a few seconds.

If the projectile must be stabilized by riding on the tube using fins or rails, the situation is worse. Fins would be partially outside the hydrogen core and would likely suffer severe ablation damage. With longitudinal rails, the vortex concept could not be used. A series of annular rails along the tube rather than longitudinal rails could provide projectile stabilization and would also allow vortex flow. An obvious disadvantage is the greatly increased complexity of the launch tube required.

Assuming longitudinal tube rails to be used, a second option might be to use a long, very thin-walled, inflatable tube in the center of the launch tube to act as a hydrogen balloon. It would be centered in the tube by the rails. Emplacing the balloon tube and filling it with hydrogen would be difficult tasks to be accomplished without causing leaks. If this could be done, however, the propellant gas fill procedure would be nearly as simple as that without a hydrogen core.

VI. Orbital Mechanics

A. Basic

Orbital mechanics for a ram accelerator space launch system has been discussed in Refs. 23 and 24. A number of points presented here, particularly the discussion of inclined orbits (see Sec. VI.C), were not treated in the earlier references. Also, a new concept, the ferry vehicle (Sec. VI.B) is presented herein. We consider as a representative ram accelerator mission to resupply a space station in a 400-km equatorial orbit. The space station is traveling eastwards and the launch will be toward the east, to take advantage of the Earth's rotation. In assessing the effects of atmospheric passage, we have used the standard atmosphere of Ref. 33, and fit it with three exponential expressions with break points at 9.6- and 47.5-km altitude. Reference 34 gives experimental drag coefficients (C_D) for small 10 deg and 5 deg half-angle cones at Mach = 15 as 0.102 and 0.071, respectively. We therefore assume $C_D = 0.10$ for the ram accelerator projectile.

We now examine the atmospheric passage and orbital requirements for the ram accelerator projectile. We integrate the equations of motion through the atmosphere and into space. From 2×10^4 to 2.6×10^6 timesteps are used to ensure good accuracy. A rotating Earth and an equatorial launch eastwards is assumed. Initially, following Refs. 23 and 24, we will consider one-impulse (11) and three-impulse (31) methods of reaching the space station (SS) orbit. We will use the following definitions. Δv is a single velocity increment provided by a rocket engine or an atmospheric passage. "Rocket Δv " is a single Δv provided by a rocket engine and Δv , is the sum of all rocket Δv s required to rendezvous at the space station. For the 11 method, when the projectile first reaches the SS orbit, a single rocket Δv is applied to place the projectile in the SS orbit. In the 31 method, the projectile is allowed to pass the SS orbit and, at apogee, a rocket Δv is applied such that the projectile will make the atmospheric passage at perigee necessary to have the new apogee at the SS orbit. A second Δv occurs on the aeropass and a small rocket Δv at the new apogee matches the projectile and SS orbits.

Figure 5a shows curves of Δv , required to rendezvous at the space station for 11 and 31 missions as a function of projectile launch velocity (v_i) and launch angle (θ). The numbers on the curves are v_i in km/s. The launch altitude is 4.5 km. The top branch of each curve (solid line) is for 11 missions and the lower branch (dashed line) is for 31 missions. The two branches meet when the projectile initial apogee is at the space station. Detailed atmospheric heating calculations were not done for the cases of Fig. 5. However, ξ , a rough measure of the total atmospheric heating load, was calculated as follows. ξ is equal to the integral of the drag force over the distance of the atmospheric passage divided by the projectile mass and the effective latent heat of vaporization of carbon (see App. C). ξ is shown in Fig. 5b as a function of v_i and θ . Heating in the 31 mission aeropass is neglected, because it is

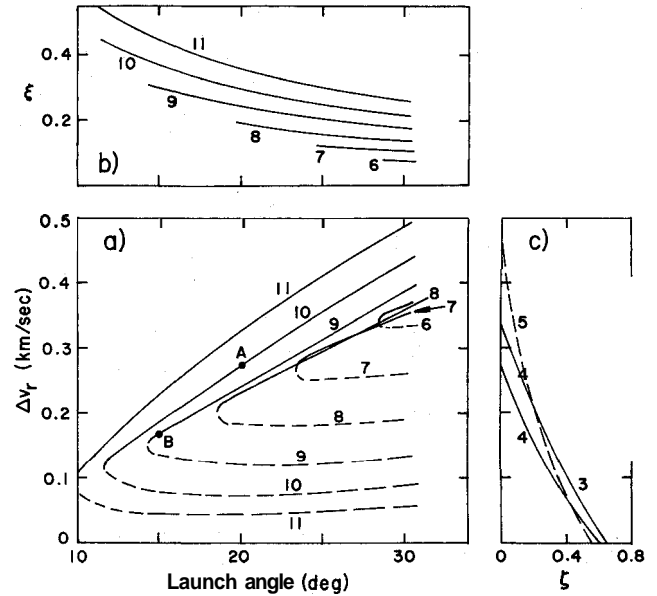


Fig. 5 a) Shows the total rocket Δv_r required to rendezvous at the space station orbit as a function of the launch velocity (v_i) and angle (θ). Numbers on curves are v_i in km/s. Curves are shown for one-impulse and three-impulse missions. The launch altitude is 4.5 km. b) Shows the dependence of total atmospheric passage heat load parameter ξ on v_i and θ . c) Shows the dependence of ζ , the ratio (net cargo gain at the space station)/(initial projectile mass), on Δv_r . Curves for three different sets of assumptions are shown. See text for details.

assumed to take place at a sufficiently slow rate that projectile material loss by ablation will be very low compared to that in the initial atmospheric passage.

We introduce a parameter, ζ , defined as (net cargo increase at the space station)/(initial ram accelerator projectile mass). Figure 5c presents three different curves for ζ as a function of Δv_r . Following Refs. 23 and 24, we have assumed a rocket exhaust velocity of 3.0 km/s. Following Ref. 24, we have assumed a ram accelerator structure mass fraction (β) of 0.3 and a ram accelerator propulsion system mass fraction (β_p) of 0.1. Curve 4 assumes the on-board propulsion system brings the entire ram accelerator projectile to rendezvous at the space station. Another possibility is that the heavy acceleration-resisting and heat-shielding components of the ram accelerator projectile could be left behind and a much lighter system comprising the propulsion system, propellants, and the cargo would rendezvous with the space station. We assume that the mass fraction of light tanks necessary to carry the propellant (and cargo, if required) (β_t) is 0.05. With these assumptions, we obtain curve 5 of Fig. 5 for $\zeta = f(\Delta v_r)$. Curve 3 will be discussed at a later point.

Let us consider a ram accelerator launch system with a given maximum v_i capability, denoted by $v_{i,m}$. Further assume that atmospheric ablation limits the maximum tolerable value of ξ to ξ_t . Let us then refer again to Fig. 5. If one chooses a 11 mission, only one rocket burn is required and there is no aeropass. The projectile propulsion and guidance systems will be relatively simple. The disadvantage is a high Δv_r , and a correspondingly low cargo mass gain (low ζ). If a 31 mission is chosen, two (or more) rocket burns and a precision aeropass (requiring accuracy within a few kilometers) are necessary. The projectile propulsion and guidance systems must be quite sophisticated. The advantage is the lower Δv_r , and higher cargo mass gained (higher ζ).

Let us consider 11 missions with a given $v_{i,m}$. If there is no limit on ξ it is always best to operate the launcher at $v_{i,m}$ to minimize Δv_r . However, with the addition of a limit on ξ , lower Δv_r s can sometimes be found for operation with $v_i < v_{i,m}$. For example, with $v_{i,m} = 10$ km/s and $\xi_t = 0.3$, if $v_i = 10$ km/s, the lowest Δv_r reachable is at point A. If $v_i = 9$ km/s, however, a significantly lower Δv_r can be found at point B.

Table 3 Net cargo increase fractions (ζ_1 and ζ_3) and optimum launch angles (θ_{10} and θ_{30}) for various $v_{l,m}$

Case	$v_{l,m}$, km/s	ζ_1	θ_{10} , deg	ζ_3	θ_{30} , deg
a	7	0.00	23.5	0.04	24
a	8	0.12	18.6	0.15	24
a	9	0.21	14.4	0.27	23
a	10	0.28	11.7	0.38	20
a	11	0.34	9.8	0.46	18
b	7	0.00	23.5	0.04	24
b	8	0.12	18.6	0.15	24
b	9	0.17	15.0	0.27	23
b	10	0.00	19.6	0.38	20
b	11	0.00	25.0	0.45	25

Curve 4 of Fig. 5c used for ζ values. Cases a with no ζ limit; cases b with $\zeta_l = 0.3$.

(Both points A and B are at $\xi = 0.3$). However, if 31 missions are considered with given $v_{l,m}$ and ξ_l , it is always best to operate at $v_{l,m}$.

For a given set of restrictions the optimum mission is defined as that with the minimum $A v$, and the consequent maximum ζ . For 11 and 31 missions, we denote the optimum launch angles by θ_{10} and θ_{30} , respectively, and the ζ values achieved by ζ_1 and ζ_3 , respectively. For the case with $v_{l,m}$ given and no restriction on ξ , Table 3, cases a give θ_{10} and θ_{30} and ζ_1 and ζ_3 for the 11 and 31 missions, respectively. With no restrictions on ξ (or, equivalently, if $\xi_l = 0.4-0.5$ is tolerable), the 11 missions are quite competitive. If, on the other hand, ξ must be limited to, as an example, $\xi_l = 0.3$, we have cases b in Table 3. For $v_{l,m}$ of 9 km/s or above ζ_1 is severely reduced from those of cases a, while ζ_3 is only slightly affected. With the addition of a limit on ξ , the optimum launch angles increase as expected.

B. Ferry Concept

In this new concept, there is an additional vehicle, the (unmanned) ferry, which leaves the space station orbit, meets the projectile, takes on board the cargo (or takes the entire projectile), and returns to the space station. The projectile alone has no maneuvering ability. This concept separates the acceleration and heat-resisting and maneuvering capabilities between the projectile and the ferry. The ferry propellant required is brought up aboard the ram accelerator projectile, in addition to the cargo to be transferred to the space station.

The main reason for considering this concept is the possibility of using totally dumb projectiles without attitude or propulsion systems. The disadvantages of the ferry concept are: first, the very existence of the ferry vehicle, which is, of course, unnecessary in nonferry ram accelerator supply missions. Second, an extremely precise matching of the ram accelerator projectile and ferry orbits is required. Third, in representative scenarios, only about 10–20 min are available for transfer of cargo from the projectile to the ferry.

To make some assessments of the ζ values achievable using the ferry concept, it is necessary to define some mass fractions for the ferry analogous to the β s for the projectile. We assume: 1) that $a = (\text{mass of ferry empty of propellant})/(\text{mass of ferry with full propellant load})$ cannot be less than 0.1, and 2) that $\alpha_f = (\text{mass of ferry empty of propellant})/(\text{initial mass of projectile to be moved by ferry} + \text{mass of ferry propellant})$ cannot be less than 0.1. These mass fractions are reasonable for a low acceleration (2–3 g at most) vehicle. For example, Ref. 35 gives a dry-to-gross-mass ratio of 0.076 for a proposed single-stage-to-orbit rocket vehicle.

Scenarios where all the propellant used is initially aboard the ferry compete quite poorly with the nonferry ram accelerator scenarios. Let us consider a scenario where the propellant for the second ferry rocket burn is brought up by the projectile and the acceleration-resisting and heat-shielding components of the projectile are left behind and only the cargo and the cargo tanks are returned to the space station.

The $\Delta v_r - \zeta$ curve for this scenario is plotted as curve 3 in Fig. 5c and is seen to be very competitive with the nonferry ram accelerator scenarios.

C. Inclined Orbits

The previous discussion of orbital mechanics has assumed an equatorial space station orbit and an equatorial ram accelerator launch. As a benchmark with equatorial orbits and launches, we compare the cargo-carrying capacity of the ram accelerator with that of the Space Shuttle. We assume 12 shuttle launches yearly with payloads of 24,900 kg. We consider a 31 ram accelerator mission with $v_l = 10$ km/s, $\theta = 20$ deg, $h_l = 4.5$ km, and a projectile mass of 2000 kg. Using Fig. 5a, we find a Δv_r of 0.72 km/s and, using the nonferry ram accelerator scenario of curve 4 in Fig. 5c, we find a net cargo increase fraction of 0.385. We define R , as the ratio of the net cargo increase rate using the ram accelerator to that using the shuttle. With the preceding scenario, if there is one launch per sidereal day, $R = 0.946$. If we assume 15 launches per day, the time between launches is roughly equal to the space station period and $R_m = 14.2$, which is very favorable.

Now, let the space station and ram accelerator launch tube orbits be inclined at 28.5 deg, the latitude of Cape Kennedy. We assume the above ram accelerator mission and assume that one launch will take place when the node lines of the ram accelerator and space station orbits coincide. Except for this launch, plane change maneuvers will be required to place the projectile in the space station orbit. The velocity requirements for these maneuvers and the consequent reduction in R_m can easily be calculated. We omit further details of the calculations, but give key results here. If there are 15 launch times per day (as in the previous example with equatorial orbits), only three of these yield any net cargo increase at the space station and R falls to 1.3. If the launch tube turnaround time can be reduced from 95.7 min (for 15 launches per day) to 11.3 min, 23 (of 127) launch times per day yield net cargo increases and R can be raised to 9.5. It may be difficult to achieve such fast launch tube turnaround times.

VII. Conclusions

The ram accelerator, a chemically driven ramjet-in-tube device is a new option for direct launch of acceleration-insensitive payloads into Earth orbit. Projectiles of masses up to several metric tons can be launched at velocities up to 10–12 km/s at nearly constant acceleration. A benchmark mission was selected: the resupply of a space station in a 400-km orbit. A number of ram accelerator drive modes were described and the above detonation velocity modes yielding the greatest theoretical acceleration capability were identified. For a space launch system, it was found that, for a number of reasons, it should be superior to stabilize the projectile in the tube by using rails on the tube rather than by fins on the projectile. However, in the former case, the flow over the forward part of the projectile is significantly affected by the rails; should this interfere with proper operation of the drive mode or cause ablation problems, fins on the projectile might be required for space launch systems.

The use of the thermally choked and above detonation velocity modes in the launch tube was compared with the use of above detonation velocity modes only; each scenario was found to have advantages and disadvantages. A preliminary study of passive stabilization using fins during atmospheric transit has indicated that this may be a viable option. Gasdynamic heating in-tube and during atmospheric transit was investigated. Heating during atmospheric transit and nose heating in-tube do not appear to cause serious mass loss problems. However, mass loss due to in-tube heating in the region of maximum pressure was found to be severe. This problem could be alleviated, however, by the use of the most suitable drive mode, transpiration cooling with NH_3 , or a hydrogen gas core in the launch tube.

The payload could be circularized in the desired orbit using one-impulse or three-impulse (with an aeropass) scenarios. The three-impulse scenarios allowed greater payload mass fractions to be placed in the final orbit, but require much more sophisticated projectile guidance and propulsion systems. A new scenario, using an auxiliary (ferry) vehicle to transport the cargo from the projectile to the space station was presented. The payload mass fraction delivered to the space station using the ferry scenario is very competitive. The ferry scenario offers the possibility of using a totally dumb projectile (without guidance, active stabilization, or propulsion systems). The ferry scenario has the disadvantages of requiring the management of second vehicle (the ferry) and requiring precision orbit matching between the projectile and the ferry.

If the orbits of the projectile and the space station are inclined at 28.5 deg (the latitude of Cape Kennedy), the cargo deliverable to the space station is reduced by a factor of ~ 10 below that for the equatorial orbits case. If a launch interval of ~ 10 min can be achieved, the ram accelerator space launch system, with 28.5-deg orbits and 2000-kg projectiles, can deliver about 10 times as much cargo to the space station as the Space Shuttle per year.

Appendix A

Simple methods for estimating the performance of the DSC and BSC modes of operation are presented here. The working gas is taken to be ideal with one set of values of molecular weight and specific heat ratio before combustion and a second set after combustion. The compression processes are approximated by two-dimensional wedge/flat-plate flows using two or four oblique shock waves. Expansions are treated isentropically. In the DSC mode, over the rear tapering part of the projectile, combustion is assumed to take place at constant pressure. If the combustion is completed before the rear tip of the projectile is reached, the flow remaining out to the rear projectile tip is taken to be an isentropic expansion. For the BSC mode, the continuity, momentum, and energy equations are solved between the flat projectile rear and an all-burnt plane aft of the projectile. The pressure at the projectile rear must be chosen to obtain a solution. The best performance is obtained when the pressure on the projectile rear is taken equal to that at the all-burnt plane. We have used these values in our comparisons in the main text. With all thermodynamic states of the cycle determined, the cycle performance parameters follow directly. As a first approximation, viscous effects reduce the performance of all modes by 10–30% and, hence, are not included here. Similar methods of analysis, but including provisions for handling normal and oblique shock waves and detonations, were used to estimate the performances of the OD1 and OD2 modes.¹⁷

Appendix B

Here, we consider the quasisinusoidal pitching motion of an axisymmetric projectile. The atmospheric density and the amplitude and the period of the pitching motion vary along the projectile path. For reasonably accurate use of the quasisinusoidal asymptotic solutions presented here, the variation of the atmospheric density and the amplitude and period of the pitching motion should not exceed roughly 10% over a period. Reference 32 (p. 322) gives the following equation for the envelope of the maximum pitch angles

$$\alpha_e(x) = \frac{C_0 \exp\left(\frac{1}{2} \int B(x) dx\right)}{[-C_{m_\alpha}(x) \rho(x) V^2(x)/2]^{.25}} \quad (B1)$$

where

$$B(x) = \frac{\rho(x)A}{2m} (\xi - C_D) \quad (B2)$$

and $\alpha_e(x)$ is the envelope of the maximum pitch angles, C_0 is a constant, x is the distance along the projectile path, $C_{m_\alpha}(x)$ is the derivative of the projectile pitching moment with respect to pitch angle, $\rho(x)$ is the atmospheric density, $V(x)$ is the projectile velocity, A is the projectile reference area, C_D is the projectile drag coefficient, and m is the projectile mass. ξ is the projectile dynamic stability parameter, which is defined in Ref. 32, p. 289.

For brevity, we replace $\rho(x)$ by p , etc. We introduce

$$\gamma = -\frac{C_{m_\alpha} V^2}{2} \quad (B3)$$

Combining Eqs. (B1), (B2), and (B3), we obtain

$$\alpha_e = \frac{C_0 \exp\left\{\int\left[\frac{\rho A}{4m}(\xi - C_D) dx\right]\right\}}{(\gamma p)^{.25}} \quad (B4)$$

We assume that $\beta = A(\xi - C_D)/(4m)$ is constant and take the atmospheric density to vary as $p = \rho_0 e^{-x/L_a}$, where ρ_0 is the atmospheric density at projectile launch and L_a is the atmospheric scale length along the projectile path. Equation (B4) then becomes

$$\alpha_e = \frac{C_0 \exp[\beta L_a(\rho_0 - \rho)]}{(\gamma \rho)^{.25}} \quad (B5)$$

As a rough approximation for a viable ram accelerator launch profile, we take $V = \text{const.}$ With this assumption, we can set

$$C_1 = \frac{C_0}{(\gamma \rho_0)^{.25}} = \text{const.} \quad (B6)$$

Combining Eqs. (B5) and (B6), we get

$$\alpha_e = \frac{C_1 \exp\left[\beta L_a \rho_0 \left(1 - \frac{\rho}{\rho_0}\right)\right]}{\left(\frac{\rho}{\rho_0}\right)^{.25}} \quad (B7)$$

The relation between the wavelength of the pitch oscillations of the projectile and the physical and aerodynamic properties of the projectile and the atmospheric density is given in Ref. 32, p. 295 as

$$C_{m_\alpha} = \frac{-8\pi^2 I}{\lambda^2 \rho A l} \quad (B8)$$

where I is the moment of inertia of the projectile for pitch oscillations, λ is the wavelength of the oscillations, and l is the reference length of the projectile. Equation (B8) can be rewritten as

$$\lambda = \left(\frac{-8\pi^2 I \rho_0}{\rho_0 A l C_{m_\alpha}}\right)^{.5} \quad (B9)$$

Finally, for quasisinusoidal motion, it is easily shown that the maximum rate of change of pitch angle $\dot{\alpha}_e$ is given by

$$\dot{\alpha}_e = \alpha_e \frac{2av}{\lambda} \quad (B10)$$

Reference 31 presents ξ , C_D , and C_{m_α} data for small 10 deg half-angle cones at Mach 15 in air. (I , A , and l data are also readily available from the reference.) We assume ξ , C_D , and C_{m_α} to be the same for the models of Ref. 31 and a large space launch projectile and we also assume geometric simi-

larity between the projectiles. Scaling for the different velocities and air densities between the model and full-scale projectiles is accounted for in Eqs. (B4), (B9), and (B10). Hence, from the data of Ref. 31, using Eqs. (B4), (B9), and (B10), and assuming an initial value of α_e , the variation of α_e , λ , and $\dot{\alpha}_e$ of the space launch projectile along its flight path can be estimated.

Appendix C

We outline here briefly the methods used to estimate the projectile ablation sustained or the transpirant required to maintain projectile integrity during launch. The first two cases studied are nose heating in-tube and during atmospheric transit. The third case is in-tube projectile sidewall heating at the point of maximum static pressure. The last case is forward cone heating during atmospheric transit. Only convective heating is considered. The projectile wall is assumed to be at 4000 K for all cases treated.

All symbols used in this appendix are defined upon first use; symbol notations used in the references have been changed as required for consistency herein. The drive modes used in the study of in-tube heating are the OD2 and BSC modes with $8\text{H}_2 + \text{O}$, as the final mixture at the tube exit. Performance reduction due to friction was included. The standard projectile (see Secs. IIIA and Fig. 2) was used, with a nose radius of 3.8 cm. For the BSC mode studies, the rear cone is omitted. In tube, given the mode, the tube fill pressure (taken as constant), the mixture at the tube exit, and the tube exit velocity, the flight profile is generated by varying the mixture in the tube to keep the projectile Mach number constant. In atmospheric transit calculations, the atmospheric density profile of Sec. VI.A was used. The flight path was simplified by assuming a flat, nonrotating Earth and a constant flight velocity and angle.

Our method of estimating nose heating starts with Eq. (1722) of Ref. 36 for the stagnation point, which is simplified by assuming a fully catalytic wall and a Lewis number of unity, yielding

$$q_{wo} = 0.66 Pr^{-2/3} \sqrt{\rho_e \mu_e} \left(\frac{du_e}{dx} \right)_s^{.5} (h_{se} - h_s) \quad (C1)$$

where q_{wo} is the heat flux, Pr is the gas Prandtl number, ρ_e , μ_e , $(du_e/dx)_s$ and h_{se} are the density, viscosity, lateral velocity gradient, and stagnation point enthalpy, respectively, at the boundary-layer edge and h_s is the enthalpy at the wall. $(du_e/dx)_s$ is estimated from Eq. (39b) of Ref. 37 as

$$(du_e/dx)_s \approx \frac{u_\infty}{r_n} \left(\frac{2\rho_\infty}{\rho_e} \right)^{.5} \quad (C2)$$

where u_∞ and ρ_∞ are the freestream velocity and density, respectively, and r_n is the nose radius. The Prandtl number is assumed to be unity and the freestream gas viscosity is assumed to vary as temperature to the 0.76 power, following van Driest.³⁸ An estimate can now be made of stagnation point heating for a smooth surface without ablation or transpiration. Reference 39 (Fig. 16) indicates that for a rough spherical surface at angles of 30–40 deg from the stagnation point, the heat transfer can be -5 times the stagnation point value. Based on this, we multiply our initial stagnation point smooth surface nonmass addition heating rate by a factor of 5.

We now correct the heating rate for surface mass addition (ablation or transpiration cooling). Reference 40 [Eq. (69) therein] gives the following algebraic correlation of experimental data for the effect of surface mass addition on heat transfer for turbulent flow over a cone.

$$\psi = \frac{q_w}{q_{wo}} = 1 - 0.29 \left(\frac{\dot{m}_e}{\dot{m}_w} \right)^{.5} B_1 + 0.015 \left(\frac{\dot{m}_e}{\dot{m}_w} \right) B_1^2 \quad (C3)$$

where q_w and q_{wo} are the heat fluxes with and without mass addition, respectively, \dot{m}_e and \dot{m}_w are the molecular weights of the shock layer and injected gas, respectively, and $B = m_w/q_{wo}(h_{se} - h_w)$, where m_w is the wall mass flux. Equation (C3) predicts negative heat transfer rates for certain values of surface mass flux, so we have fit the data of Ref. 40 with the following exponential expression which avoids this difficulty:

$$\psi = \exp \left[-0.391 \left(\frac{\dot{m}_e}{\dot{m}_w} \right)^{\delta} B_1 \right] \quad (C4)$$

Reference 40 has used the grouping $(\dot{m}_e/\dot{m}_w)^{.5} B$, in Eq. (C3) to account for the molecular weight effect in the foreign gas surface mass addition. Upon examination of Jeromin's data⁴¹ on the effect of foreign gas injection on skin friction and wall heating rates, we found, instead, a dependence on molecular weight to the -0.67 power. Hence, we use $\delta = 0.67$ instead of $\delta = 0.5$ in Eq. (C4). Using the above procedures to estimate the nose heat flux as a function of nose mass flux and the conservation of energy equation at the nose wall, the nose heat and mass fluxes can be calculated. To complete the calculation, one must have values for the molecular weight (\bar{M}) of the mass addition gases and the effective latent heat of vaporization (L_v) of the ablatant or transpirant. Here, L_v is calculated as the energy per gram to raise the wall material or transpirant from 300 K as a solid or liquid to a gas at 4000 K. Carbon was assumed to evaporate to C, and NH_3 and H, were assumed to evaporate to equilibrium mole fraction mixtures at 4000 K and representative pressure levels. For NH_3 and H_2 transpirants, the nose radius was taken as 3.8 cm and was fixed. The total transpirant required was obtained by integrating the mass flux over the flight profile and multiplying by the nose area. For C ablation, the nose radius was allowed to increase progressively during ablation.

For forward cone atmospheric transit heating, heating rates and wall mass fluxes are calculated at a number of points along the flight profile and integrated to give the total consumption of ablatant or transpirant. For in-tube sidewall heating at the point of maximum pressure, the heating rate and wall mass flux are calculated at the tube exit condition and a simple scaling law, presented later, is used to account for the varying velocity and gas composition along the in-tube flight profile. For the condition in question, the skin friction coefficient without mass addition is calculated using Eq. (71) of Ref. 42, as follows:

$$\frac{0.242}{A(C_{f_{x0}})^{.5}(T_w/T_\infty)^{.5}} (\sin^{-1} \alpha + \sin^{-1} \beta) = \log_{10}(R_\infty C_{f_{x0}}) - \frac{1 + 2\omega}{2} \log_{10} \frac{T_w}{T_\infty} \quad (C5)$$

where $C_{f_{x0}}$ is the mean skin friction coefficient, T_w and T_∞ are the wall and freestream static temperatures, respectively, R_∞ is the Reynolds number based on freestream conditions, and ω is the viscosity-temperature exponent. We have used $\omega = 0.76$, following Ref. 38. In Eq. (C5)

$$\alpha = \frac{2A^2 - B}{(B^2 + 4A^2)^{.5}} \quad \text{and} \quad \beta = \frac{B}{(B^2 + 4A^2)^{.5}}$$

and

$$A^2 = \frac{\frac{\gamma - 1}{2} M_\infty^2}{T_w/T_\infty} \quad \text{and} \quad B = \frac{1 + \frac{\gamma - 1}{2} M_\infty^2}{T_w/T_\infty} - 1$$

where γ and M_∞ are the freestream specific heat ratio and Mach number, respectively.

The effect of mass addition is calculated using the equation of Fig. 8 of Ref. 43, which can easily be transformed to yield the following equation:

$$\frac{C_{fz}}{C_{fz0}} = \frac{1}{\left[1 + 3.83 \frac{m_w}{\rho_\infty u_\infty} \left(\frac{\rho_\infty}{\rho^*} \right)^{.5} \left(\frac{2}{C_{fz0}} \right)^{.5} \left(\frac{C_{fz0}}{C_{fz}} \right)^{.25} \right]^3} \quad (C6)$$

where C_{fz} and C_{fz0} are the skin friction coefficients with and without mass addition, respectively, and ρ^* is the density of the freestream gas at the reference temperature, T^* . We evaluate the reference temperature using Eq. (25) of Ref. 43 with the last term dropped, as follows:

$$T^* = 0.5(T_w + T_\infty) + 0.2(T_r + T_\infty) \quad (C7)$$

where T_r is the recovery temperature. We have approximated $T_r = T_\infty + 0.5u_\infty^2/C_p$ where C_p is the specific heat at constant pressure of the freestream gas. We have multiplied the $m_w/(\rho_\infty u_\infty)$ term of Eq. (C6) by $(\bar{m}_e/\bar{m}_w)^{.67}$ to account for the effect of foreign gas mass addition following Jeromin's data,⁴¹ as described above. Using Reynolds' analogy⁴⁴ and the conservation of energy equation at the wall, we can calculate the skin friction coefficient, the heat transfer rate, and the wall mass flux. Again, carbon ablation and NH_3 and H_2 transpiration cooling were considered.

For atmospheric heating on the forward cone, the forward cone "freestream" condition was approximated as that behind the oblique shock on a wedge with half-angle two-thirds that of the cone. The total mass losses were then calculated by integrating over the flight profile and multiplying by the forward cone area. The severity of carbon ablation was also assessed by calculating the wall retreat, dr , divided by the maximum projectile radius, r . The in-tube sidewall heat flux (q_w) and the wall mass flux (\dot{m}_w) at the point of maximum pressure were calculated at the maximum in-tube velocity. To integrate over the in-tube flight profile, we use the approximation that $q_w \propto \dot{m}_w \propto \rho_1 u_1^3 C_{fz}$ where ρ_1 is the density just upstream of the projectile and u_1 is the projectile velocity. For our in-tube flight profiles, $\rho_1 u_1^2$ and C_{fz} are roughly constant. The integration of \dot{m}_w over the flight profile then becomes very simple. The total mass loss per unit area follows directly. For NH_3 and H_2 transpirants, the total quantity of transpirant required follows by multiplication by the relevant surface area of the projectile. For C ablation, the final result will also be given as the wall retreat, dr , divided by the maximum projectile radius, r .

Acknowledgments

This research was supported by Grant NCC-2-487 from NASA to the Elore Institute. The author wishes to acknowledge a number of very helpful conversations with M. E. Tauber and A. P. Bruckner.

References

- ¹Bruckner, A. P., "A Gun-Launched Satellite," *Spaceflight*, Vol. 7, 1965, pp. 118-121.
- ²Eder, D., "A Low Cost Earth Based Launch System and its Effect on Space Industrialization," *Space Manufacturing 4: Proceedings of the 5th Conference*, Princeton, NJ, May 18-21, 1981, pp. 221-229.
- ³O'Neill, G. K., "The Colonization of Space," *Physics Today*, Vol. 27, 1974, pp. 32-40.
- ⁴Chilton, F., Hibbs, B., Kolm, H., O'Neill, G. K., and Phillips, J., "Electromagnetic Mass Drivers," *Progress in Aeronautics and Astronautics*, Vol. 57, 1917, pp. 37-61.
- ⁵Barber, J. P., "Direct Launch Using the Electric Rail Gun," *Proceedings of the JANAF Propulsion Meeting*, Vol. 1, 1983, pp. 51-56.
- ⁶Kolm, H., Mongeau, P., Fitch, O., Williams, F., Graneau, P., and McKinney, K., "An Electromagnetic First Stage Cargo Launcher," *Space Manufacturing 4: Proceedings of the 5th Conference*, Princeton, NJ, May 18-21, 1981, pp. 231-233.
- ⁷Hawke, R. S., Brooks, A. L., Fowler, C. A., and Peterson, D.

- R., "Electromagnetic Railgun and Launchers: Direct Launch Feasibility," *AIAA Journal*, Vol. 20, July 1982, pp. 978-985.
- ⁸Winterberg, F., "The Electromagnetic Rocket Gun," *Acta Astronautica*, Vol. 12, 1985, pp. 155-161.
- ⁹Miller, L. A., Rice, E. E., Earhart, R. W., and Conlon, R. J., "Preliminary Analysis of Space Mission Applications for Electromagnetic Launchers," Final Technical Rept., Contract NAS 3-23354, Battelle Columbus Laboratories, Columbus, OH, Aug. 30, 1984.
- ¹⁰Wilbur, P. J., Mitchell, C. E., and Shaw, B. D., "The Electrothermal Ramjet," *Journal of Spacecraft and Rockets*, Vol. 20, Nov.-Dec. 1983, pp. 603-610.
- ¹¹Glumb, R. J., and Krier, H., "Concepts and Status of Laser Supported Rocket Propulsion," *Journal of Spacecraft and Rockets*, Vol. 21, Jan.-Feb. 1984, pp. 70-79.
- ¹²Huberman, M., Sellen, J. M., Benson, R., Davenport, W., Davidheiser, R., Molmod, P., and Glatt, L., "Investigation of Beamed Energy Concepts for Propulsion," AFRPL-TR-76-66, Oct. 1976, p. 113.
- ¹³Kare, J. T., ed., "Proceedings of the SDIO/DARPA Workshop on Laser Propulsion, Lawrence Livermore National Laboratory, 7-18 July 1986, Vol. 1—Executive Summary," CONF-860778, Lawrence Livermore National Laboratory, CA, Nov. 1986.
- ¹⁴Powers, M. V., Zaretsky, C., and Myrabo, L. N., "Analysis of Beamed Energy Ramjet/Scramjet Performance," AIAA Paper 86-1761, AIAA/SAE/ASME/ASEE 22nd Joint Propulsion Conf., Huntsville, AL, June 16-18, 1986.
- ¹⁵Hertzberg, A., Bruckner, A. P., and Bogdanoff, D. W., "Ram Accelerator: A New Method of Accelerating Projectiles to Ultrahigh Velocities," *AIAA Journal*, Vol. 26, Feb. 1988, pp. 195-203.
- ¹⁶Bruckner, A. P., Bogdanoff, D. W., Knowlen, C., and Hertzberg, A., "Investigation of Gasdynamic Phenomena Associated with the Ram Accelerator Concept," AIAA Paper 87-1327, AIAA 19th Fluid Dynamics, Plasma Dynamics and Lasers Conf., Honolulu, HI, June 8-10, 1987.
- ¹⁷Knowlen, C., Bruckner, A. P., Bogdanoff, D. W., and Hertzberg, A., "Performance Capabilities of the Ram Accelerator," AIAA Paper 87-2152, AIAA/SAE/ASME/ASEE 23rd Joint Propulsion Conference, San Diego, CA, June 29-July 2, 1987.
- ¹⁸Brackett, D. C., and Bogdanoff, D. W., "Computational Investigation of Oblique Detonation Ramjet-in-Tube Concepts," *Journal of Propulsion and Power*, Vol. 5, No. 3, May-June, 1989, pp. 276-281.
- ¹⁹Bruckner, A. P., Knowlen, C., Scott, K. A., and Hertzberg, A., "High Velocity Modes of the Thermally Choked Ram Accelerator Concept," AIAA Paper 88-2925, AIAA/SAE/ASME/ASEE 24th Joint Propulsion Conf., Boston, MA, July 11-13, 1988.
- ²⁰Yungster, S., and Bruckner, A. P., "A Numerical Study of the Ram Accelerator Concept in the Superdetonative Velocity Range," AIAA Paper 89-2677, AIAA/ASME/ASEE Joint Propulsion Conf., Monterey, CA, July 10-12, 1989.
- ²¹Kull, A. E., Burnham, E. A., Knowlen, C., Bruckner, A. P., and Hertzberg, A., "Experimental Studies of Superdetonative Ram Accelerator Modes," AIAA Paper 89-2632, AIAA/SAE/ASME/ASEE 25th Joint Propulsion Conf., Monterey, CA, July 10-12, 1989.
- ²²Burnham, E. A., Kull, A. E., Knowlen, C., Bruckner, A. P., and Hertzberg, A., "Operation of the Ram Accelerator in the Transdetonative Velocity Range," AIAA Paper 90-1985, AIAA/SAE/ASME/ASEE 26th Joint Propulsion Conf., Orlando, FL, July 16-18, 1990.
- ²³Bruckner, A. P., and Hertzberg, A., "Ram Accelerator Direct Launch System for Space Cargo," Paper IAF-87-211, 38th Congress of the International Astronautical Federation, Oct. 10-17, Brighton, U.K.
- ²⁴Kaloupis, A., and Bruckner, A. P., "The Ram Accelerator: A Chemically Driven Mass Launcher," AIAA Paper 88-2968, 24th AIAA/ASME/SAE/ASEE Joint Propulsion Conf., Boston, MA, July 11-13, 1988.
- ²⁵Hogg, I. V., *The Guns 1939-45*, Ballantine Books, New York, 1970, pp. 127, 130.
- ²⁶Kerrebrock, J. L., *Aircraft Engines and Gas Turbines*, Massachusetts Institute of Technology Press, Cambridge, MA, 1977, pp. 105-107.
- ²⁷Shapiro, A. H., *The Dynamics and Thermodynamics of Compressible Fluid Flow*, Ronald, New York, 1953, pp. 135-136.
- ²⁸Kepler, C. E., Debois, R. L., and Spadacini, L. J., Patent 4,726,279, Feb. 23, 1988.
- ²⁹Lord, M. E., "Performance of a 40-mm Combustion Heated Light Gas Gun Launcher," Arnold Engineering Development Center Rept., AEDC-TN-60-176, Oct. 1960.
- ³⁰Waldrom H. F., McMahan, H. M., and Letarte, M., "Free Flight

Facilities and Aerodynamic Studies at Canadian Armament Research and Development Establishment," IAS Paper 60-90, Presented at the IAS National Summer Meeting, Los Angeles, CA, June 28-July 1, 1960.

³¹Intrieri, P. F., Kirk, D. B., Chapman, G. T., and Terry, J. E., "Ballistic Range Tests of Ablating and Non-Ablating Slender Cones," *AZAA Journal*, Vol. 8, March 1970, pp. 558-564.

³²Canning, T. N., Seiff, A., and James, C. S., "Ballistic Range Technology," AGAR DGraph No. 138, Aug. 1970.

³³Shapiro, A. H., op. cit., pp. 612-613.

³⁴Strawa, A. W., and Prabhu, D. K., "A Comparison of Experimental and Computational Results for 5 and 10 Degree Cones at High Mach Numbers," Paper AIAA-88-2705, Presented at the AIAA Thermophysics, Plasmadynamics and Lasers Conf., San Antonio, TX, June 27-29, 1988.

³⁵Martin, J. A., Nattel, J. C., and Turriziani, R. V., "Propulsion Evaluation for Orbit-on-Demand Vehicles," *Journal of Spacecraft and Rockets*, Vol. 23, Nov.-Dec. 1986, pp. 612-619.

³⁶Schreier, S., *Compressible Flow*, Wiley, New York, 1982, p. 436.

³⁷Tauber, M. E., "A Review of High-speed Convective Heat-Transfer Computational Methods," NASA Technical Paper 2914, July 1989, p. 6.

³⁸van Driest, E. R., "Turbulent Boundary Layer in Compressible Fluids," *Journal of Aeronautical Sciences*, Vol. 18, March 1951, p. 153.

³⁹Tauber, M. E., op. cit., p. 15.

⁴⁰Ibid., p. 19.

⁴¹Jeromin, L. O. F., "The Status of Research in Turbulent Boundary Layers with Fluid Injection," *Progress in Aeronautical Sciences*, Vol. 10, 1970, pp. 153-162.

⁴²van Driest, E. R., op. cit., p. 154.

⁴³Knuth, E. L., and Dershin, H., "Use of Reference States in Predicting Transport Rates in High-speed Turbulent Flows with Mass Transfer," *International Journal of Heat Mass Transfer*, Vol. 6, 1963, pp. 999-1018.

⁴⁴Shapiro, A. H., op. cit., pp. 1100-1101.

**Recommended Reading from the AIAA
Progress in Astronautics and Aeronautics Series . . .**



Spacecraft Dielectric Material Properties and Spacecraft Charging

Arthur R. Frederickson, David B. Cotts, James A. Wall and Frank L. Bouquet, editors

This book treats a confluence of the disciplines of spacecraft charging, polymer chemistry, and radiation effects to help satellite designers choose dielectrics, especially polymers, that avoid charging problems. It proposes promising conductive polymer candidates, and indicates by example and by reference to the literature how the conductivity and radiation hardness of dielectrics in general can be tested. The field of semt-insulating polymers is beginning to blossom and provides most of the current information. The book surveys a great deal of literature on existing and potential polymers proposed for noncharging spacecraft applications. Some of the difficulties of accelerated testing are discussed, and suggestions for their resolution are made. The discussion includes extensive reference to the literature on conductivity measurements.

TO ORDER. Write, Phone, or FAX: American Institute of Aeronautics and Astronautics c/o Publications Customer Service 9 Jay Gould Ct., P O Box 753, Waldorf MD 20604 Phone 301/645 5643 or 1-800/682-AIAA, Dept 415 ■ FAX 301/843-0159

Sales Tax CA residents 8 25%. DC. 6% For shipping and handling add \$4 75 for 1-4 books (call for rates for higher quantities) Orders under \$50 00 must be prepaid Foreign orders must be prepaid Please allow 4 weeks for delivery Prices are subject to change without notice Returns will be accepted within 15 days

1986 96 pp., illus. Hardback
ISBN 0-930403-17-7
AIAA Members \$29.95
Nonmembers \$37.95
Order Number V-107